Ray Tracing Animated Scenes using Coherent Grid Traversal

Ingo Wald　　　Thiago Ize　　　Andrew Kensler　　　Aaron Knoll　　　Steven G. Parker

SCI Institute, University of Utah,　50 S Central Campus Dr., Salt Lake City, UT, 84112
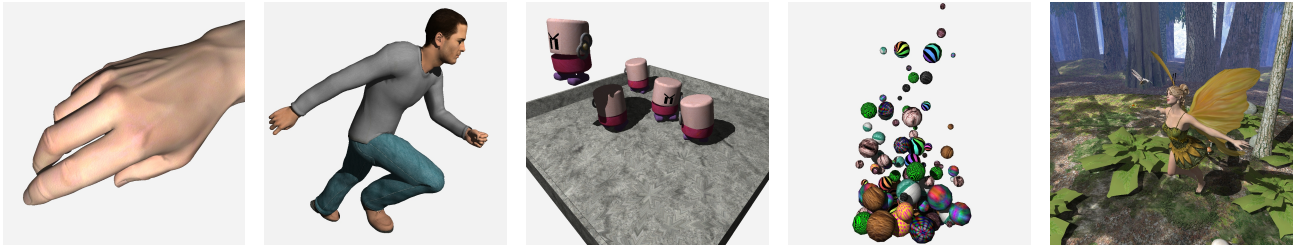
Figure 1: Several animated models ray traced using our coherent grid traversal: a) A gesturing hand of 16K triangles. b) An animated "Poser" model (78K triangles). c) Animated wind-up toys (11K triangles) walking and jumping incoherently around each other. d) A rigid-body dynamics simulation of marbles (8.8K triangles). e) A complex scene of 174K animated triangles, where a fairy and a dragonfly dance through an animated forest. Scenes are rebuilt from scratch every frame, allowing fully dynamic animation. Including shading, texturing, and hard shadows, as used in the above images, we can render these scenes at 1024×1024 pixels with 15.3, 7.8, 10.2, 26.2, and 1.4 frames per second on a dual 3.2 GHz Xeon. Excluding shading, texturing, and shadows, we achieve 34.5, 15.8, 29.3, 57.1, and 3.4 frames per second.

Abstract

We present a new approach to interactive ray tracing of moderate-sized animated scenes based on traversing frustum-bounded packets of coherent rays through uniform grids. By incrementally computing the overlap of the frustum with a slice of grid cells, we accelerate grid traversal by more than a factor of 10, and achieve ray tracing performance competitive with the fastest known packet-based kd-tree ray tracers. The ability to efficiently rebuild the grid on every frame enables this performance even for fully dynamic scenes that typically challenge interactive ray tracing systems.

1　Introduction and Related Work

Over the last 20 years, a number of different data structures have been proposed for accelerating ray tracing, such as Bounding Volume Hierarchies (BVH), Grids, Octrees [Glassner 1984], and Binary Space Partitioning (see, e.g., [Glassner 1989; Havran 2001]). Each of these data structures has its own strengths and weaknesses, and the effectiveness of each technique strongly depends on the scene, application, and efficiency of the actual implementation. Recent work in interactive ray tracing, however, has focused primarily on kd-trees [Wald 2004; Foley and Sugerman 2005; Reshetov et al. 2005; Woop et al. 2005] and grids [Purcell et al. 2002], or multilevel grids [Parker et al. 1999b; Reinhard et al. 2000].

While the first interactive ray tracers used grids [Parker et al. 1999b], algorithmic developments for kd-tree based ray tracers — most notably coherent ray tracing [Wald et al. 2001] and MLRT traversal [Reshetov et al. 2005] — have significantly improved the performance of kd-trees. Packet tracing creates groups of spatially coherent rays that are simultaneously traced *together* through a kd-tree, where all rays perform each traversal iteration in lock-step. This enables effective use of SIMD extensions on modern CPUs, increases the computational density of the code, and reduces strain on memory access. In turn, this gave rise to fast software implementations [Wald 2004], and to instruction-parallel special-purpose ray tracing hardware [Woop et al. 2005]. Exploiting the coherence in a packet of rays has yielded further improvements in "Multilevel Ray Tracing" (MLRT) [Reshetov et al. 2005], where a bounding frustum drives the kd-tree traversal of rays in bulk instead of considering each ray individually. Consequently, the cost of a traversal step becomes independent of the number of rays in the packet, encouraging larger packets with significantly lower cost per ray.

Unfortunately, these techniques are not directly applicable to grids. Thus, packet-enabled kd-trees have recently consistently outperformed grid-based ray tracers, and many believe that they are a superior acceleration structure (see, e.g., [Stoll 2005]).

Dynamic Scenes　Although packet kd-tree traversals outperform grids for static scenes, animated scenes present a challenge due to the high cost of rebuilding a kd-tree as objects move. For the surface area heuristics required to build fast kd-trees [Wald and Havran 2006], building the acceleration structure effectively requires seconds to minutes for moderately complex scenes. This limitation to static scenes limits the utility of interactive ray tracing for many applications that would benefit from advanced lighting models, such as visual simulation, animations, and interactive games. While some efforts have focused on extending kd-trees to dynamic scenes [Wald et al. 2003; Günther et al. 2006], they are limited to mostly hierarchical motion or require advance knowledge of the scene, and therefore are unsuitable for most truly dynamic animations that require unstructured motion. For full generality, we propose rebuilding the acceleration structure from scratch every frame. For general scenes, with kd-trees this is currently infeasible.

A grid, in contrast, can be created and modified at interactive rates [Reinhard et al. 2000], at least for moderate sized scenes of up to a few hundred thousand triangles. Consequently, grids are attractive for dynamic scenes because of their faster build, even if they have a higher traversal cost than a kd-tree. Nevertheless, as kd-trees can be up to an order of magnitude faster than single-ray grids, grids will only be viable when their traversal can be performed with similar efficiency. Ultimately, this will require employing the same techniques for grids that made kd-trees as fast as they are today: coherent packets of rays, SIMD, and frusta. However, the 3D digital differential analyzer algorithms usually used for traversing a grid do not lend well to packetization, as we will explain below.

In this paper, we propose a new traversal scheme for grid-based acceleration structures that allows for traversing and intersecting packets of coherent rays using an MLRT-inspired frustum-traversal scheme. This algorithm is well-suited for SIMD implementation and provides dramatic speedup over a conventional grid traversal, yielding performance comparable to kd-tree based systems for static scenes. More importantly, this scheme facilitates animated scenes in a straightforward manner by interactively rebuilding the grid from

scratch every frame. Using this technique on a fully animated teapot-in-a-stadium stress scene of 174K triangles, we achieve a ray tracing performance of around 1-2 frames per second (at 1024^2 pixels with hard shadows and simple shading) on a dual 3.2 GHz Xeon CPU; for a 16K triangle object, we achieve 15-16 fps (Figure 1). We mostly consider moderate scenes of up to a few hundred thousand triangles, and focus on only primary and shadow rays.

The importance of supporting dynamic scenes has recently been recognized by many different researchers, and several different approaches have been proposed concurrently to our work, for example [Wald et al. 2006; Stoll et al. 2006; Günther et al. 2006; Lauterbach et al. 2006]. We will compare to these approaches in Section 5.

2 Coherent Grid Traversal

Efficient ray-grid traversal has already received much attention [Cleary et al. 1983; Fujimoto et al. 1986; Amanatides and Woo 1987; Parker et al. 1999b; Spackman and Willis 1991], in aspects of both algorithm and implementation. Significant improvements cannot be expected from merely optimizing current implementations; we must explore new concepts to design an effective packetized traversal. Our new algorithm delivers to grids the same components that made kd-trees as fast as they are today: packets, SIMD extensions, and frustum traversal; while preserving the trivial computation of an incremental grid marching step.

In this section, we explain why these techniques have been successful for other acceleration structures and discuss the difficulties of applying the same concepts to a conventional grid traversal. Then, we derive our new packet traversal scheme, and show how it can benefit from known optimizations to achieve significantly higher performance than past grid implementations.

2.1 Issues with Packetized Grids

The basic idea of packet and frustum traversal is straightforward: rather than traverse each ray on its own, we exploit the intrinsic coherence between neighboring rays, and trace them together. If the rays are coherent, they will largely traverse the same regions of space, accessing identical nodes in an acceleration structure, and intersecting the same underlying triangles. Effectively, the cost of memory access becomes amortized over all the rays in a packet, ideally for both our acceleration structure and geometry data. In addition, traversing multiple rays through the same node of the acceleration structure allows us to perform SIMD operations on four rays at once, reducing the computation costs of both traversal and primitive intersection by up to a factor of four. Finally, frustum techniques determine intersection patterns of an entire packet, often replacing intensive per-ray branching with a single test; thus amortizing the computations over the entire packet.

The advantages of packets, SIMD, and frustum methods are beneficial to any acceleration structure. Spatially hierarchical structures, such as a kd-tree or BVH, typically exhibit little divergence at the upper levels of traversal, making them ideally suited for adaptation to ray packets. Packets are easily traversed through hierarchical acceleration structures where rays generally progress through identical cells; diverging only in finer nodes deep down in the hierarchy, if at all. Even when rays diverge, some rays just traverse a few cells that they would not have traversed otherwise, but do not interfere with traversal decisions in the remaining part of the subtree. Since the packet is never divided, those rays automatically are re-enabled as soon as the recursion returns from that subtree.

For a grid, in contrast, the situation is more complicated: traversal is always performed on the same fine level, where divergence is most likely. Moreover, grid based ray tracers typically use 3D digital differential analyzers (3DDDA) or Bresenham-like algorithms to iterate through the voxels traversed by the ray (e.g., [Fujimoto et al.

1986; Amanatides and Woo 1987; Spackman 1990]). These algorithms can chose only one cell at a time to step into, but different rays can disagree on the next cell to be traversed. For example, Figure 2 shows five rays diverging in cell B; some demand traversal to C, while others demand traversal to D. If the packet decides to go to C first, the 3DDDA state variables for those rays entering cell D become invalid (and vice versa). These invalid state variables break the 3DDDA algorithm in the next traversal step.

This disagreement could be solved by splitting the packet into subpackets with the same traversal decision. However, Figure 2 shows that the rays that have diverged in cell B still traverse other common cells (E and F) later on. If the packet were split at cell B, that coherence would be lost; in practice, packet splitting quickly deteriorates to single-ray traversal. Re-merging the packets after each step would solve that problem, but is prohibitively expensive.
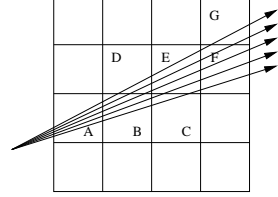

Figure 2: Five coherent rays traversing a grid. The rays are initially together in cells A and B, but then diverge at B where they disagree on whether to first traverse C or D in the next step. Even though they have diverged, they still visit common cells (E and F) afterwards.

2.2 A Slice-based Packet Traversal for Grids

As the above discussion has shown, the primary concern with packetizing a grid is that with a 3DDDA, different rays may demand different traversal orders. We solve this by abandoning 3DDDA altogether, and devise an algorithm that traverses the grid *slice by slice* rather than cell by cell. For example, we can traverse the rays in Figure 2 by traversing through vertical slices; from cell A in the first slice, we would traverse the rays to cells B and D in the second slice, then to C and E in the third, and so on. In each slice, we would intersect all rays with all of the slice's cells that are overlapped by any ray. This may traverse some rays through cells they would not have intersected themselves, but will keep the packet together at all times. In Figure 2, we would intersect 7 cells with 5 rays each, instead of 27 cell visits if the rays are traced individually. Though the packet now intersects only 7 instead of 27 cells, the total number of ray-cell intersection tests is $7 \times 5 = 35$. In practice, ray coherence easily compensates for this overhead.

We first transform the rays into the canonical grid coordinate system, in which a grid of $N_x \times N_y \times N_z$ cells maps to the 3D region of $[0..N_x) \times [0..N_y) \times [0..N_z)$. In that coordinate system, the cell coordinates of any $3D$ point p can be computed simply by truncating it. Then, we pick the dominant component (the $\pm X$, $\pm Y$, or $\pm Z$ axis) of the direction of the first ray. This will be the *major traversal axis* that we call $\vec{K}$; all rays are then traversed along this same axis; the remaining dimensions are denoted $\vec{U}$ and $\vec{V}$. In order to traverse the rays front to back, which allows early termination when all rays have intersected before the next slice, all rays must have the same sign along the traversal direction. For coherent packets, this is not a limitation; to violate this assumption, two rays would need to span an angle of more than $\frac{\pi}{2}$. Note that we do *not* demand that all rays in a packet have the same dominating axis, nor that their direction signs match along $\vec{U}$ or $\vec{V}$, as is usually required by kd-tree packet traversers [Wald 2004] as long as the rays are coherent.

Now, consider a slice k along the major traversal axis, $\vec{K}$. For each ray r_i in the packet, there is a point p_i^{in} where it enters this slice, and a point p_i^{out} where it exits. The axis aligned box $\mathcal{B}$ that

encloses these points will also enclose all the $3D$ points — and thus, the cells — visited by at least one of of the rays. Once $\mathcal{B}$ is known, truncating its min/max coordinates yields the u, v extents of all the cells on slice k that are overlapped by any of the rays (Figure 3d).
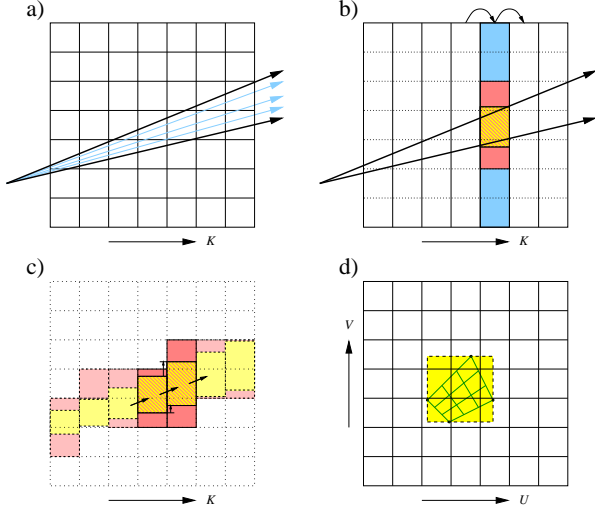

Figure 3: Given a set of coherent rays, our algorithm first computes the packet's bounding frustum (a) that is then traversed through the grid one slice at a time (b). For each slice (blue), we incrementally compute the frustum's overlap with the slice (yellow), which determines the actual cells (red) overlapped by the frustum. (c) Independent of packet size, each frustum traversal step requires only one four-float SIMD addition to incrementally compute the min and max coordinates of the frustum slice overlap, plus one SIMD float-to-int truncation to compute the overlapped grid cells. (d) Viewed down the major traversal axis, each ray packet (green) will have corner rays which define the frustum boundaries (dashed). At each slice, this frustum covers all of the cells covered by the rays.

Extension to Frustum Traversal Instead of determining the overlap $\mathcal{B}$ based on the entry and exit points of *all* rays, we can compute the four planes bounding the packet on the top, bottom, and sides. This forms a bounding frustum that has the same overlap box $\mathcal{B}$ as that computed from the individual rays[1]. Since the rays are already transformed to grid-space, we can determine our bounding planes based on the minima and maxima of all the rays' u and v slopes along $\vec{K}$. For a packet of $N \times N$ primary rays, we can simply compute these extremal planes using the four corner rays; however for more general (secondary) packets all rays must be considered.

Traversal Setup Once the plane equations are known, we can intersect the frustum with the bounding box of the grid; the minimum and maximum coordinates of the overlap determine the first and last slice that should be traversed. If this interval is empty, the frustum misses the grid, and we can terminate without traversing.

Otherwise, we compute the minimum and maximum u and v coordinates of the entry and exit points with the first slice to be computed. Essentially, these describe the lower left and upper right corner of an axis-aligned box bounding the frustum's overlap with the initial slice, $\mathcal{B}^{(0)}$. Note that we only need the u and v coordinates of each $\mathcal{B}^{(i)}$, as the k coordinates are equal to the slice number.

Incremental Traversal Since each slice's overlap box $\mathcal{B}^{(i)}$ is determined by the frustum's planes, the minimum and maximum coordinates of two successive boxes $\mathcal{B}^{(i)}$ and $\mathcal{B}^{(i+1)}$ will differ by a constant vector $\Delta\mathcal{B}$. With each slice being 1 unit wide, this $\Delta\mathcal{B}$ is simply $\Delta\mathcal{B} = (du_{min}, du_{max}, dv_{min}, dv_{max})$, where the

$du_{min/max}$ and $dv_{min/max}$ are the slopes of the bounding planes in the grid coordinate space.

Given a slice's overlap box $B^{(i)}$, we can now incrementally compute the next slice's overlap box $B^{(i+1)}$ via $B^{(i+1)} = B^{(i)} + \Delta B$. This requires only four floating point additions, and can be performed with a single SIMD instruction. As mentioned above, once a slice's overlap box B is known, the range $[i_0..i_1] \times [j_0..j_1]$ of overlapped cells can be determined by truncating $\mathcal{B}$'s coordinates and converting them to integer values. This operation can also be performed with a single SIMD float-to-int conversion instruction. Thus, for arbitrarily sized packets of $N \times N$ rays, the whole process of computing the next slice's overlapped cell coordinates costs only two instructions: one SIMD addition, and one SIMD float-to-int conversion. The complete algorithm is sketched in Figure 3.

2.3 Efficient Slice and Triangle Intersection

Once the cells overlapped by the frustum have been determined, we intersect all of the rays in a packet with the triangles in each cell. Triangles may appear in more than one cell, and some rays will traverse cells that would not have been traversed without packets. Consequently, redundant triangle intersection tests are performed. The overhead of these additional tests can be avoided using two well-known techniques: SIMD frustum culling and mailboxing.

SIMD Frustum Culling A grid does not conform as tightly to the geometry as a kd-tree, and thus requires some triangle intersections that a kd-tree would avoid (see Figure 4). To allow for interactive grid builds, cells are filled if they contain the bounding boxes of triangles rather than the triangles themselves, further exacerbating this problem (see Section 3). However, as one can see in Figure 4, many of these triangles will lie completely outside the frustum; had they intersected the frustum, the kd-tree would have had to perform an intersection test on them as well.
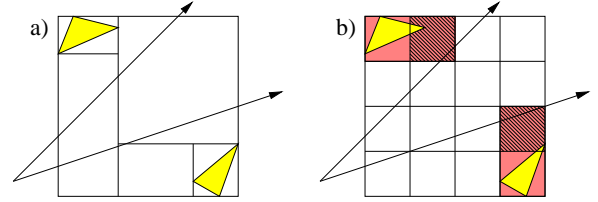

Figure 4: Since a grid (b) does not adapt as well to the scene geometry as a kd-tree (a), a grid will often intersect triangles (red) that a kd-tree would have avoided. These triangles however usually lie far outside the view frustum, and can be inexpensively discarded by inverse frustum culling during frustum-triangle intersection.

For a packet tracer, triangles outside the bounding frustum can be rejected quite cheaply using Dmitriev et al.'s "SIMD shaft culling" [2004]. If the four "corner rays" of the frustum miss the triangle on the *same* edge of the triangle, then all the rays must miss that triangle[2]. Using the SIMD triangle intersection method outlined in [Wald 2004], intersecting the four corner rays costs roughly as much as a single SIMD 4-ray-triangle intersection test. As such, for an N-ray packet, triangles outside the frustum can be intersected at $\frac{4}{N}$ the cost of those inside the frustum.

Mailboxing In a grid, large triangles may overlap many cells. In addition, since a single-level grid cannot adapt to the position of a triangle, even small triangles often straddle cell boundaries. Thus, most triangles will be referenced in multiple cells. Since these references will be in neighboring cells, there is a high probability that our frustum will intersect the same triangle multiple times. In

---

[1]This is similar in spirit to beam tracing [Heckbert and Hanrahan 1984].

[2]Note that some (virtual) corner rays can also be computed for other than primary rays, by taking the four edges of the bounding frustum.

fact, as shown in Figure 5 this is much more likely for our frustum traversal than for a single-ray traversal: While a single ray would visit the same triangle only along one dimension, the frustum is several cells wide, and will re-visit the same triangle in all three dimensions.
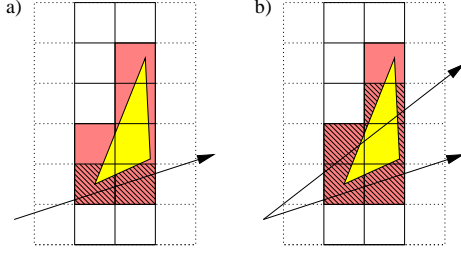

Figure 5: While one ray (a) can re-visit a triangle in multiple cells only along one dimension, a frustum (b) visits the same triangle much more often (even worse in 3D). These redundant intersection tests would be costly, but can easily be avoided by mailboxing.

Repeatedly intersecting the same triangle can be avoided by mailboxing [Kirk and Arvo 1991]. Each packet is assigned a unique ID, and a triangle is tagged with that ID before the intersection test. Thus, if a packet visits a triangle already tagged with its ID, it can skip intersection. Mailboxing typically produces minimal performance improvement in either a grid or a kd-tree for inexpensive primitive such as triangles; and may even reduce performance if gains from avoiding repeat intersection tests do not outweigh the costs of checking and updating the mailbox [Havran 2002].

As explained above, however, our frustum grid traversal yields far more redundant intersection tests than a single ray grid or kd-tree, and thus profits better from mailboxing. Additionally, the overhead of mailboxing for a packet traverser becomes insignificant; the mailbox test is performed *per packet* instead of per ray, thus amortizing the cost as we have seen before.

Impact of Mailboxing and Frustum Culling Mailboxing and frustum culling are both very useful in reducing the number of redundant intersection tests. In fact, both methods are much more powerful for our frustum grid traversal than for their original applications. Mailboxing is performed for multiple rays simultaneously, so the cost is amortized over the entire packet, and also avoids more redundant intersection tests. Similarly, due to the higher number of redundant triangle intersections in the packetized grid, SIMD frustum culling is more beneficial than in a kd-tree, where these intersections may have been avoided in the first place.

To quantify the magnitude of this impact, we have measured statistics on example scenes, using OpenRT's kd-tree system employing 4×4 packets, and our frustum grid also using 4×4 packets. For each of those, we have measured the total number of ray-triangle intersections that are performed if neither of these techniques are used, then the results when mailboxing and finally SIMD frustum culling are applied. As can be seen from Table 1, mailboxing alone reduces the number of tests by up to a factor of 2; for a kd-tree, it usually trims this by less than 10% [Havran 2002]. On top of the reductions achieved by mailboxing, frustum culling achieves yet another reduction by a factor of 4 to 9. With both techniques, the final number of intersection tests decreases by a factor of 8.5 to 14, and the absolute number of ray-triangle intersection tests roughly matches that of a kd-tree (see Table 1).

Together, mailboxing and frustum culling remedy the deficiencies of frustum traversal on uniform grids. Only one source of overhead cannot be avoided: when the bounding box of a triangle overlaps some cells traversed by a ray, but does not fall entirely outside the frustum. This scenario, however, is not limited to the grid; it also occurs in a packetized kd-tree.

scene	#tris	grid			grid ratio	kd-tree
	MB/FC	n/n	y/n	y/y	n/n to y/y	
toys	11K	14.0M	8.7M	1.0M	14.0	0.82M
hand	15K	12.5M	6.0M	0.9M	13.9	0.85M
ben	78K	12.8M	6.0M	1.5M	8.5	1.1M
conf	274K	96.0M	54M	6.9M	13.9	3.7M

Table 1: Ray-triangle intersection tests for a 4×4 kd-tree and for our 4×4 frustum-grid traversal, and the impact of using mailboxing (MB) and frustum culling (FC). Mailboxing and frustum culling reduce the number of ray-triangle intersections by up to a factor of 14, to roughly as few as performed by a good kd-tree.

2.4 Extension to Hierarchical Grids

Our algorithm so far has been described for a single-level grid; however hierarchical grids generally achieve superior performance. There are several ways to organize grids hierarchically, including loosely nested grids [Cazals et al. 1995; Klimaszewski and Sederberg 1997], recursive or multiresolution grids [Jevans and Wyvill 1989], and macrocells or multigrids [Parker et al. 1999a]. Though these terms are ill-defined and often used ambiguously, they all share the same idea of subdividing some regions of space more finely than others, and thus traverse empty space more quickly than populated space. To demonstrate that our approach is not restricted to uniform grids, we have extended it with a single-level macrocell layer. Macrocells are a simple hierarchical optimization to a base uniform grid, often used to apply grids to scalar volume fields [Parker et al. 1999a]. Macrocells superimpose a second, coarser grid over the original fine grid, such that each macrocell corresponds to an $M \times M \times M$ block of original grid cells. Each macrocell stores a boolean flag specifying whether any of its corresponding grid cells are occupied.

Building the macrocell grid is trivial and cheap. Traversing it with our algorithm is rather simple: the macrocell grid in essence is just an $M \times M \times M$ downscaled version of the original grid, and many of the values computed in the frustum setup can be re-used, or computed by dividing by M. During traversal, we first consider a slice of macrocells, and determine all the macrocells overlapped by the frustum (usually but one in practice). If the macrocells in our slice are all empty, we can skip M traversal steps on our original fine grid. Otherwise, we perform these steps as usual.

Though the best value of M obviously depends on the scene, $M = 6$ has consistently shown to be a good choice for the test scenes in our system. For smaller resolutions, the savings for each macrocell step become too small to justify the additional computations; for larger resolutions the probability of finding empty regions decreases. Using macrocells yields a performance improvement of around 30%, which is consistent with improvents seen for single ray grids. Additional levels of macrocells could further improve performance for more complex models with larger grids. More robust varieties of hierarchical grids could speed up large scenes with varying geometric density, at the cost of higher build time. As our goal is to formulate a viable grid traversal for medium-size animated scenes, these have not yet been investigated.

3 Acceleration Structure Rebuild

With an animated scene, our acceleration structure is recreated every frame. Though schemes for incrementally [Reinhard et al. 2000] or hierarchically [Lext and Akenine-Möller 2001] updating a grid exist, we did not want to impose any restrictions on the kind of animations we support, and thus opted for the most general method by rebuilding the grid from scratch for every frame. We use the common scheme of choosing the number of cells to be a multiple, λ, of the number of triangles, N [Cleary et al. 1983]. Due to having the smallest surface area in relation to volume, cubically shaped cells minimize a grid's expected ray tracing cost. Thus, we choose the
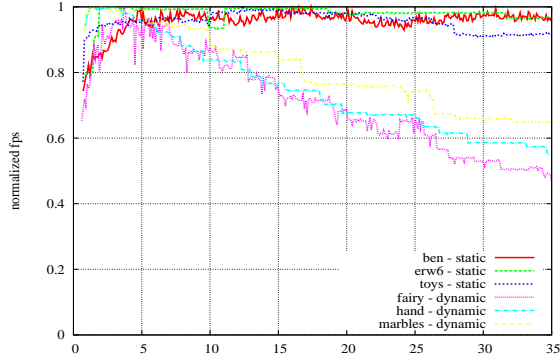
Figure 6: For several different models, this graph shows the framerate, normalized by the best time, in relation to grid size as determined by λ (on the X axis). Nearly all tested scenes, both static and dynamic, reach their optimum at approximately $\lambda \approx 5$.

grid's resolution as:

$$N_x = d_x \sqrt[3]{\frac{\lambda N}{V}}, N_y = d_y \sqrt[3]{\frac{\lambda N}{V}}, N_z = d_z \sqrt[3]{\frac{\lambda N}{V}},$$

where $\vec{d}$ is the diagonal and V the volume of our grid. Fortunately, our experiments show that most scenes are insensitive to the parameter λ and achieved their best performance around $\lambda = 5$ (Figure 6), which we use for all the experiments throughout this paper.

Once the grid resolution is chosen, for each triangle we determine the cells overlapped by the triangle's bounding box and add a reference to the triangle to each of these cells. Since this is quite conservative, we also tested a more exact grid insertion scheme using an exact triangle-in-box test (e.g., [Akenine-Möller 2001]). Though the exact test could reduce the number of triangle references in the grid by more than one third, the number of ray-triangle intersection tests after mailboxing would shrink by only a few percent. For such a small gain, the significantly higher rebuild cost does not pay off, leading us to use the less accurate — but faster — bounding box test. For scenes with dominantly long, skinny, and diagonal triangles, a more accurate test may still pay off.

Since memory allocations are costly, we use a preallocated pooled-memory scheme that prevents per-cell memory allocations and fragmentation as the scene changes from frame to frame. We also use the macrocell information from the previous frame to reduce the number of cells we need to check for objects to clear. Memory layout techniques such as bricking [Parker et al. 1999b] have also been tested; but since the frustum traversal already amortizes memory accesses over the entire packet, these techniques did not result in a measurable performance difference for our scenes. Larger grids, however, may still benefit from these techniques.

In addition to rebuilding the grid, we also need to create the derived data for the triangle test described in [Wald 2004]. Though this could be avoided by storage-free triangle tests [Möller and Trumbore 1997], we found these to be slightly inferior in performance even after per-frame triangle rebuild time is taken into account; again, this could be different for much larger scenes than we tested. Furthermore, the triangle rebuild takes less time than the grid rebuild, and can be run in parallel with the grid rebuild.

4   Experiments and Results

In addition to the statistics presented above, we evaluated the performance of our algorithm on a working implementation. We first discuss the impact of the different governing parameters, and present performance for both static and dynamic scenes. If not mentioned otherwise, all experiments are performed at 1024×1024 pixels, without display, and on a dual 3.2 GHz Intel Xeon PC.

4.1   Impact of Grid and Packet Resolution

For any given scene, the performance of our frustum traversal algorithm is governed by four factors: The resolution of the grid, macrocell resolution, screen resolution, and ray packet size. As shown in the previous section, choosing the grid resolution via $\lambda = 5$ in practice works fine for the kind of moderate-sized scene we are targeting. Similar experiments show that a macrocell resolution of $6 \times 6 \times 6$ usually yields reasonable performance. Though tweaking these parameters can result in additional performance gains, these default parameters usually work well.

While grid and macrocell resolution do have an impact, screen resolution and packet size have the greatest impact on performance. For any given packet size, the cost of a traversal step is constant, but the cost for intersecting the cells in a slice increases with the number of cells that the frustum overlaps. Larger packets will benefit more from the constant cost traversal step, but are also more likely to overlap more cells. Thus, there is a natural crossover point where the savings in traversal steps from a larger packet are offset by the additional cell intersections. Obviously, this crossover point will be influenced by the model resolution, as larger models have finer grids and correspondingly smaller cells.

To find that crossover point — and thus determine the optimal packet size — we generated different resolutions of the Stanford Armadillo model and measured the rendering performance for packets of 2×2, 4×4, 8×8, 16×16, and 32×32 rays per packet. The results of these experiments are given in Figure 7. For 2×2 rays, the benefit of tracing packets is rather small, and the rendering times correspondingly high. Also not surprisingly, for packets of 32×32 rays, the frusta get very wide and performance deteriorates quickly as model complexity increases. Packets of 16×16 rays are better, but still deteriorate quite quickly. For small to medium sized models, 8×8 packets performed best until the crossover point of 250k triangles, at which point the smaller 4×4 packets begin to work better for large models. If a higher degree of coherence is given for a certain application — for example for higher resolutions, multiple samples per pixel for antialiasing or motion blur, or when computing soft shadows with lots of shadow rays to the same light source — even larger packets can still be beneficial.
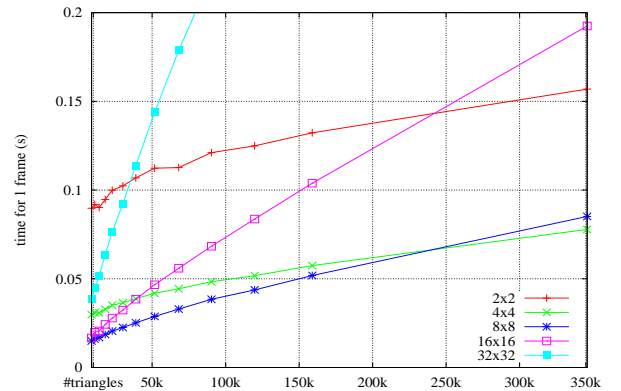

Figure 7: Static render time with varying packet sizes and different resolutions of the Stanford Armadillo. There is a crossover point around 250K triangles where 4×4 packets become more efficient than 8×8 packets. Nevertheless, both 4×4 and 8×8 show nearly the same performance over a wide range of model complexity.

4.2   Scalability with Screen Resolution

Obviously, the optimal packet size also depends on the screen resolution, as higher resolutions result in a higher density of rays, and thus allow for larger packet sizes. Given today's hardware constraints, we chose 1024×1024 pixels as a default resolution for all our experiments. In the future, high-resolution displays and supersampling

will push demand for even larger images.

While the cost of ray tracing is usually considered to be linear in the number of pixels, this is not the case for our algorithm. Since higher resolutions enable larger packets, we generally see sublinear scaling in screen resolution: When increasing the screen resolution from 1024×1024 to 2048×2048 the frame rate usually drops by only a factor of 1.75-2.25, significantly less than the expected factor of 4. Weakening the linear dependence on pixel count helps overcome a major hurdle in interactive ray tracing systems.

4.3 Performance for Static Scenes

Though our main motivation was to enable ray tracing of dynamic scenes, the performance gains achieved by the packet traversal apply also to static models. To evaluate our raw ray tracing performance, we used several typical static test models for ray tracing, and rendered them with our system with the rebuild disabled. This lets us consider traversal time independently from grid build time, and facilitates a comparison between our algorithm and contemporary interactive ray tracing systems, namely OpenRT [Wald 2004] and Intel's MLRT system [Reshetov et al. 2005].

For this comparison, we chose the erw6, conference, and soda hall scenes of 800, 280K, and 2.2M triangles, respectively, as these are the only scenes for which numbers from both systems are available [Reshetov et al. 2005]. Though the axis-aligned features of these three architectural models strongly favor the kd-trees used in MLRT and OpenRT, Table 2 shows that our system, despite relatively little low-level optimization, is competitive even for these best-case scenarios for the other systems, usually being around 3-4× slower than MLRT, but consistently faster than OpenRT.

scene	#tris	OpenRT Pentium IV 2.5 GHz	MLRT Pentium IV 3.2 GHz w/ HT.	Frustum Grid Pentium IV 3.2 GHz w/ HT
erw6	804	2.3	50.7	18.3
conf	274k	1.93	15.6	4.0
soda hall	2.2m	1.8	24.1	8.0

Table 2: Static scene ray tracing performance for both the packetized grid, OpenRT, and MLRT. OpenRT and MLRT data are taken from [Reshetov et al. 2005]; all times are including simple shading, but without display. Though these three scenes are best-case examples for our competitors, we remain at least competitive.

4.4 Scalability with Model Resolution

As shown in Section 3, for moderate-sized scenes as targeted in our system, the optimal grid resolution is usually near $\lambda \approx 5$. For significantly larger models of up to several million triangles, however, the time for building a fine grid may no longer pay off for the constant number of rays shot, and a coarser grid may yield the higher aggregate performance if build time is taken into account. As shown in Figure 8, for the 10 million triangle Thai Statue, the grid rebuild for $\lambda = 5$ already takes three times longer than tracing the rays. In that case, trading grid resolution for lower rebuild times pays off, reaching the optimal aggregate performance around $\lambda = 1$. Though the thus reduced grid resolution increases the render time, this is more than made up for in saved rebuild time, resulting in a total rendering time *including* rebuild of less then 1.5s per frame. This

time can be further reduced using a second thread for the rebuild, which we do not want to discuss here in detail.

For comparison, for the Soda Hall model the grid at $\lambda = 1$ can be rebuilt (using one build thread only) in a mere 110ms, and achieves a frame rate (including rebuild) of 3.5 frames/second; i.e., even including rebuild, the full 2.2M triangle model is still interactive. Though this shows that a coarser grid can pay off for much larger models than intended for our technique, in the remainder of this paper we will use the above-mentioned default resolution of $\lambda = 5$.
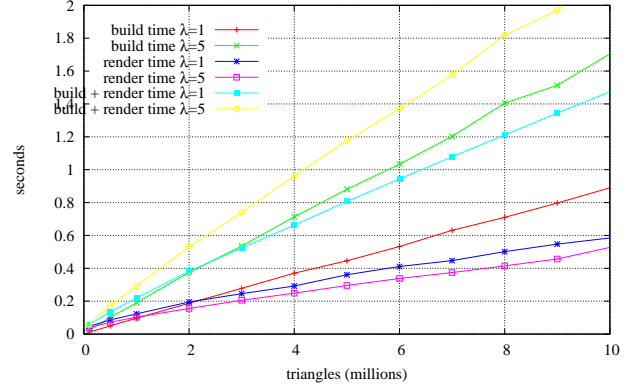

Figure 8: Rebuild and render times at $\lambda = 1$ and $\lambda = 5$ for different resolutions of the Stanford Thai Statue ranging from 100K to 10M triangles. For these large models, we use a packet size of 4×4.

4.5 Comparison to Single-Ray Grid Traversal

The somewhat surprising performance of our frustum grid on architectural models can be explained by the benefits of packetization. To illustrate this difference, we compare our approach to an optimized single-ray 3DDDA implementation of a hierarchical grid. Though this implementation uses a more sophisticated multilevel hierarchy, Table 3 shows that the packetized grid ranges from 6 to 21 times faster, depending on the scene and viewpoint. Though some of this improvement is due to our use of SIMD extensions that cannot easily be used with single-ray traversal, SIMD implementation alone usually gives only about a factor of two; the remainder is due to cost amortizations and the algorithmic improvements of the packet/frustum technique.

scene	ben	hand	toys	erw6	conf
single-ray	1.57	1.59	1.53	0.67	0.30
8×8 packets	10.6	16.1	20.0	14.0	3.2
ratio	6.75	10.1	13.1	20.9	10.6

Table 3: Static scene performance (in frames per second) for our system; and for an optimized 3DDDA single-ray grid, using a macrocell hierarchy if advantageous. Images rendered at 1024×1024 pixels on a Pentium IV 3.2 GHz CPU with 1 thread and simple shading. Our frustum traversal outperforms the single-ray variant by up to an order of magnitude.

This effect can best be explained by the number of cells visited during traversal: as we see in Table 4, compared to a single ray traversal, the frustum version visits roughly 10 to 20 times fewer cells for the 4×4 packets, and over 50 times fewer for the 8×8 packets. Due to efficient packetized slice and triangle intersection (Section 2.3), the frustum actually tests fewer triangle intersections as well; and can even do that in SIMD.

scene	ben	hand	toys	erw6	conf
# ray-triangle intersection tests (millions)					
single ray	2.96	3.58	1.97	8.90	15.70
packet 4×4	1.50	0.93	1.02	1.54	6.90
packet 8×8	5.74	2.54	2.23	2.00	20.70
# visited cells (millions)					
single ray	24.30	19.60	7.72	33.20	167.70
packet 4×4	2.91	0.95	0.80	2.18	16.54
packet 8×8	1.37	0.36	0.32	0.58	5.84
ratio 4×4	13.10	20.74	9.65	15.23	10.13
ratio 8×8	8.35	54.90	23.9	55.7	28.70

Table 4: Total number of triangles intersected and cells visited (in millions) for a single ray grid; a 4×4; and an 8×8 packet traversal. No macrocells are being used by either grid, and tests use identical dimensions for the same scene. Frustum traversal dramatically reduces both the numbers of cell visits and triangle intersection tests.

4.6 Performance for Animated Scenes

To support animation, the simplest mechanism for a grid is to rebuild the grid structure every time the geometry changes. For small to medium sized scenes, rebuilding the grid is fast; allowing the performance achieved for static scenes to be sustained during animation. For larger scenes, other techniques such as incremental or parallel rebuilds may be required to maintain interactive performance, although these techniques were not employed here. To demonstrate these performance characteristics, we used several animated scenes of various sizes and different dynamic behavior, and measured the rebuild time and rendering performance.

Animated meshes   Some of the benchmark scenes are depicted in Figure 9: The "wood-doll" is a simple model with 5k triangles, resulting in a grid of $18 \times 48 \times 36$ cells that can be built in 1ms. Without shading, this scene can be rendered at 67 frames per second; even including shading and shadows, 35 frames per second can be reached. However, consisting only of rigid body animation of its otherwise static limbs, the wood-doll could also be rendered using rigid-body animation schemes for kd-trees as proposed in [Wald et al. 2003].

To stress more complex kinds of animation, we also tested an animated "hand" model of 16K triangles, as well as "ben", a runner character of 80K triangles. Though the "ben" model is already non trivial in size, its grid of $48 \times 108 \times 78$ cells can be rebuilt in only 14ms, resulting in a final performance of 16fps without shading, and 9fps with shading and shadows turned on. The "hand" ($72 \times 36 \times 36$ cells built in 5ms) can be rendered at 36 and 16 frames per second, respectively.
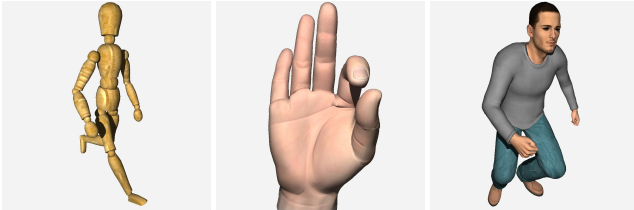

Figure 9: Some of the simpler animated models: a rigid-body wood-doll (5.3k triangles), a gesturing hand (16k triangles), and a running poser figure (78k triangles). Without shading and shadows, these scenes render at 66.9, 35.9, and 16.3 frames per second (including grid rebuild), and still at 35.1, 15.9, and 8.9 frames per second with shading, texturing, and shadows turned on.

Non-hierarchical animation   Though differing in their forms of animation, both "wood-doll", "hand", and "ben" are individual models that are tightly enclosed by the grid. To demonstrate that our method is not limited to such models, the "toys" scene has a set of 5 individually animated wind-up toys that walk around incoherently, bump into each other, and even jump over each other (see Figure 10). With a total of 11K triangles, grid rebuild (for $66 \times 18 \times 66$ cells) took 4ms, yielding a frame rate of 9-17 and 28-40fps with and without shading and shadows, respectively.

The grid's strongest advantage over other dynamic data structures is that it does not require any kind of a hierarchy to be present in the model. Thus, it can also be used for completely incoherent motion of triangles, such as explosions, physics-driven simulations, or particle sets. To demonstrate this, we modelled a scene where 110 "marbles" are dropped into a (invisible) glass box, where they participate in a rigid-body simulation (Figure 10). Since the grid does not depend on any kind of coherence in the motion, this kind of animation can be supported easily, taking just 2ms to rebuild ($24 \times 78 \times 24$ cells), and rendering at 20-24 respectively 42-50fps.
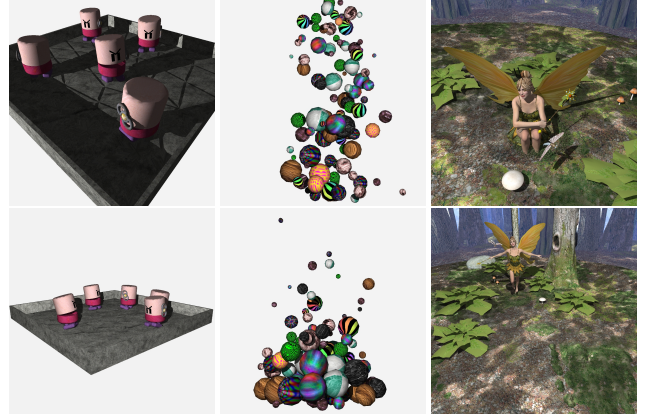

Figure 10: Examples of complex scenes composed of multiple individual objects: a) wind-up toys walking around and colliding with each other (11K tri); b) A simulation of 110 marbles dropping into an (invisible) box (8.8K tri). c) A complex scene of a typical game scenario: A skinned fairy and dragonfly dance through an animated forest (174K tri total). For the camera and light positions shown, these animations respectively run at 28.0/39.6, 41.5/50.2, and 3.3/4.3 fps without shading, and still at 9.4/17.3, 19.6/24.2, and 1.3/1.8 fps if shading, texturing, and shadows are turned on.

A real-world example   While all these scenes are more or less artificial test models, the "fairy forest" scene (see Figure 10) has been chosen in particular because of its similarity to typical interactive scenarios: In this scene, a fairy and a dragonfly dance through an animated forest; both fairy and dragonfly are animated via a skinned skeleton. The scene incorporates both locally dense and largely empty regions; it is rather wide in spatial extent, requires complex shading, and consists of a total of 174K triangles, most of which are animated. Initially, we expected the high variation in scene density to be quite a challenge for our approach. However, the frustum traversal did surprisingly well, and still achieved some 3-4 and 1-2fps for shading and no shading, respectively. The fairy's grid of $150 \times 42 \times 150$ cells can be rebuilt in 68ms.

The scenes discussed above were all modeled offline as animation sequences. This fact is not exploited at all by our traverser. The grid itself is built from a list of triangles and vertex positions every frame, neither knowing nor caring where they originate. It does not exploit the temporal coherence properties of sequenced animation, but therefore also does not depend on it. Thus, the system would work just as well for completely dynamic models. The number of triangles in the scene can easily be changed from frame to frame, and there is no restriction on the movement of existing triangles.

4.7 Shading, Shadows, and secondary Rays

So far all results have considered primary rays only. However, the true beauty of ray tracing — and its main advantage over algorithms like Z-Buffering — is that it can employ secondary rays to compute effects such as shadows, reflections, and refraction.

Among all kinds of secondary rays, shadow rays are arguably the easiest one, as they usually expose the amount of coherence that packet and frustum-based techniques like ours depend on. For most rendering algorithms, coherent shadow rays can be generated by connecting all of the primary rays' hit points to the same point light source [Wald et al. 2001]. Though certain algorithms like Monte Carlo path tracing [Kajiya 1986]), can exhibit incoherence even in shadow rays, most practical applications of ray tracing produce coherent shadow rays, and even global illumination has already been demonstrated with such rays [Benthin et al. 2003].

If we connect all surface hit points to the same point light source, the resulting shadow packets share a common origin just like primary rays, and differ from those only in that they have no concept of "corner rays". However, one can easily determine a principal march direction of the packet, and can then construct a frustum over the packet by determining the four planes that tightly bound the rays along that direction. The four edges of this frustum can then be determined quite cheaply, and can be used to perform the SIMD frustum marching and SIMD frustum culling.

Though shadow packets often *are* coherent, there is no guarantee that this is *always* the case. For example, if a primary packet hits an object's silhouette, the 3D hitpoints can be quite distant from each other, and connecting them to the same point light yields a wide frustum for which our method breaks down. In fact, for a frustum-based technique like ours the impact of some packets getting incoherent is much worse than for pure packet-based techniques, as all the triangles in the frustum would get intersected, which might comprise large parts of the scene.

Fortunately, however, this case can be detected and alleviated quite easily as already proposed in [Wald et al. 2001]: If the primary hit points are too far apart (measured, for example, by the minimum and maximum hit distances along the packet), the packet can be split into two more coherent subpackets. Without packet splitting, certain scene and light configurations can easily lead to severe performance degradation for shadows; while with splitting, shadow rays in practice work just as well as primary rays.

More general packets that do not even share the same origin would also be possible, as long as the rays are still coherent. Initial experiments have shown that this works quite well when, for example, computing soft shadows by connecting multiple surface samples with multiple light samples on the same light source. Though packet/frustum-based systems have shown that reflection and refraction rays often work surprisingly well in packet-based renderers [Woop et al. 2005; Mahovsky 2005], no experimental data are available for our coherent frustum traversal technique, yet.

5 Summary and Discussion

We presented a new approach to ray tracing with uniform grids. This algorithm elegantly allows for transferring the recent advantages in fast ray tracing — namely, ray packets, frustum testing and SIMD extensions — to grids, for which these techniques had previously not been available. The frustum based grid traversal has several important advantages. First, it has a simple traversal step, where a few SIMD operations allow for determining all the cells in a grid slice that are overlapped by the frustum. This operation has a constant cost for the entire frustum that is amortized over the entire packet of rays, and allows for a traversal step that is at least as cheap as that of a packet/frustum kd-tree. Using mailboxing and SIMD frustum culling (Section 2.3), our method performs roughly

the same number of ray-triangle intersection tests as the kd-tree. Though our implementation is not *as* highly tuned as that of Intel's MLRT system [Reshetov et al. 2005], it is up to 21 times faster than known single-ray grid traversal schemes; competitive with kd-trees; and inherently supports fully-dynamic animated scenes.

Our method does possess several limitations. The very nature of using a uniform grid makes the method ill-suited for highly complex scenes with a high variation in size and density of geometry; for example, the Boeing 777 data set or the classic teapot-in-a-stadium. Though our macrocell technique works for most cases, for highly complex scenes multiresolution grids [Parker et al. 1999b], multi-level techniques [Wald 2004; Lext and Akenine-Möller 2001], or separation of static and dynamic objects [Reinhard et al. 2000], as well as mechanisms to incrementally rebuild the grid data structure may be advantageous.

Grids still suffer from common pathological cases such as large flat areas (i.e., from architectural models) where geometry overlaps numerous cells. These situations can be handled more efficiently by today's kd-tree based ray tracers and therefore, kd-trees are likely to remain somewhat more efficient for many scenes. It is also not guaranteed that our technique will perform similarly well for other kinds of secondary rays like reflection and refraction, for which the coherence can be lower than for primary and shadow rays.

Our technique may be very appropriate for special-purpose hardware architectures such as GPUs and the IBM Cell processor [Minor et al. 2005] that offer several times the computational power of our current hardware platform. Though kd-trees have been realized on both architectures, they are limited by the streaming programming model in those architectures. In contrast, a grid-based iteration scheme is a better match to these architectures, and may be able to achieve a higher fraction of their peak performance. The current method may also be appropriate for a hardware-based implementation, similar to Woop et al. [2005].

The primary motivation of this approach is to enable ray tracing of dynamically deforming models. Rebuilding an acceleration structure on each frame enables ray tracing these models without placing any constraints on the motion. As this update cost is — like rasterization — linear in the number of triangles, it introduces a natural limit for the size of models that can be rebuilt interactively. The rebuild cost is manageable for many applications such as visual simulation or games, where moderate scene sizes with several thousand to a few hundred thousand polygons are common.

Comparison to Alternative Approaches In this paper, we have shown that uniform grids are a viable option for interactively ray tracing animated scenes. Nevertheless, other alternatives exist: Even without any assumptions on the scene structure, today's $O(N \log N)$ kd-tree construction schemes in practice exhibit near-linear complexity [Wald and Havran 2006], albeit with higher constants; thus, kd-tree construction could eventually be optimized to achieve interactive rebuilds. As soon as some assumptions on the scene can be made, even more alternatives become available: If information from the scene graph could be exploited to steer the building process [Stoll et al. 2006], interactive kd-tree rebuilds may become feasible. For the case of locally smooth animations whose deformations are known in advance, Günther et al. [2006] have proposed to cluster the triangles into groups of similarly moving triangles, the motion of which is decomposed into a rigid-body transform and a residual motion, which are then handled separately. For a similar class of scenes — albeit with fewer a-priori knowledge of the deformation — Wald et al. have also proposed an approach based on merely deforming a bounding volume hierarchy [Wald et al. 2006]: Using a specially designed traversal scheme their dynamic BVH performs competitively to both grids and kd-trees. All these approaches allow for interactively ray tracing animated scenes, and more competitors are likely to appear. Hybrid approaches (e.g., a

kd-tree for static content and one separate grid for each animated character) may be possible, but this has not yet been investigated.

From the performance and efficiency standpoint, among all these approaches our coherent grid traversal is arguably the most extreme one in that it is a *pure* frustum-based technique, while all other approaches are mixed packet/frustum-traversal techniques (i.e., [Reshetov et al. 2005; Günther et al. 2006; Wald et al. 2006]). Compared to a packet-based technique, a pure frustum traversal can take even better benefit from coherence *if* it exists; for example, though doubling the number of rays in the packet would increase the total number of ray-triangle intersections, the *traversal* cost would not change at all. On the other hand, with rising incoherency a pure frustum based technique will deteriorate much more quickly than the other techniques — a single incoherent ray in a packet can significantly widen a frustum, and lead to painfully degraded performance. Similarly, the frustum alone is prone to suffer worse from triangles becoming smaller: In the worst case, the frustum will intersect all the triangles in the frustum, even if those become as small as to fall in between the raster of rays in the packet. Consequently, when comparing our approach to, for instance, the BVH-based packet/frustum technique described in [Wald et al. 2006] we typically see that both techniques usually are within a factor of $\sim 2\times$ within each others performance; the BVH usually has a slight advantage — in particular for increasingly complex scenes — but can suffer worse for intentionally designed worst-case scenes, and in addition is less general in the kind of scenes it can handle.

In summary, we believe our approach to be at least competitive with other data structures and traversal algorithms known today, while at the same time being the most general of these techniques, supporting any incoherent deformation to the scene.

Acknowledgments

References

AKENINE-MÖLLER, T. 2001. Fast 3D triangle-box overlap testing. *J. Graph. Tools 6* (1), 29–33.

AMANATIDES, J., AND WOO, A. 1987. A Fast Voxel Traversal Algorithm for Ray Tracing. In *Eurographics '87*. Eurographics Association, 3–10.

BENTHIN, C., WALD, I., AND SLUSALLEK, P. 2003. A Scalable Approach to Interactive Global Illumination. *Computer Graphics Forum 22* (3), 621–630. (Proceedings of Eurographics).

CAZALS, F., DRETTAKIS, G., AND PUECH, C. 1995. Filtering, Clustering and Hierarchy Construction: a new solution for Ray Tracing very Complex Environments. In *Proceedings of Eurographics '95*.

CLEARY, J., WYVILL, B., BIRTWISTLE, G., AND VATTI, R. 1983. A Parallel Ray Tracing Computer. In *Proceedings of the Association of Simula Users Conference*, 77–80.

DMITRIEV, K., HAVRAN, V., AND SEIDEL, H.-P. 2004. Faster Ray Tracing with SIMD Shaft Culling. Research Report MPI-I-2004-4-006, Max-Planck-Institut für Informatik, Saarbrücken, Germany.

FOLEY, T., AND SUGERMAN, J. 2005. KD-tree acceleration structures for a GPU raytracer. In *Proceedings of HWWS*, 15–22.

FUJIMOTO, A., TANAKA, T., AND IWATA, K. 1986. ARTS: Accelerated ray tracing system. *IEEE CG&A 6* (4), 16–26.

GLASSNER, A. S. 1984. Space subdivision for fast ray tracing. *IEEE CG&A 4* (10), 15–22.

GLASSNER, A. 1989. *An Introduction to Ray Tracing*. Morgan Kaufmann.

GÜNTHER, J., FRIEDRICH, H., WALD, I., SEIDEL, H.-P., AND SLUSALLEK, P. 2006. Ray tracing animated scenes using motion decomposition. In *Proceedings of Eurographics 2006*. (to appear).

HAVRAN, V. 2001. *Heuristic Ray Shooting Algorithms*. PhD thesis, Faculty of Electrical Engineering, Czech Technical University in Prague.

HAVRAN, V. 2002. Mailboxing, Yea or Nay? *Ray Tracing News 15* (1).

HECKBERT, P. S., AND HANRAHAN, P. 1984. Beam tracing polygonal objects. In *Proceedings of SIGGRAPH*, 119–127.

JEVANS, D., AND WYVILL, B. 1989. Adaptive voxel subdivision for ray tracing. *Proceedings of Graphics Interface '89* (June), 164–172.

KAJIYA, J. T. 1986. The Rendering Equation. In *Computer Graphics (Proceedings of ACM SIGGRAPH)*, D. C. Evans and R. J. Athay, Eds., vol. 20, 143–150.

KIRK, D., AND ARVO, J. 1991. Improved ray tagging for voxel-based ray tracing. In *Graphics Gems II*, J. Arvo, Ed. Academic Press, 264–266.

KLIMASZEWSKI, K. S., AND SEDERBERG, T. W. 1997. Faster ray tracing using adaptive grids. *IEEE CG&A 17* (1) (Jan./Feb.), 42–51.

LAUTERBACH, C., YOON, S.-E., TUFT, D., AND MANOCHA, D. 2006. RT-DEFORM: Interactive Ray Tracing of Dynamic Scenes using BVHs. Tech. Rep. 06-010, Department of Computer Science, University of North Carolina at Chapel Hill.

LEXT, J., AND AKENINE-MÖLLER, T. 2001. Towards rapid reconstruction for animated ray tracing. In *Eurographics Short Presentations*, 311–318.

MAHOVSKY, J. 2005. *Ray Tracing with Reduced-Precision Bounding Volume Hierarchies*. PhD thesis, University of Calgary.

MINOR, B., FOSSUM, G., AND TO, V. 2005. TRE : Cell broadband optimized real-time ray-caster. In *Proceedings of GPSx*.

MÖLLER, T., AND TRUMBORE, B. 1997. Fast, minimum storage ray triangle intersection. *JGT 2* (1), 21–28.

PARKER, S., PARKER, M., LIVNAT, Y., SLOAN, P.-P., HANSEN, C., AND SHIRLEY, P. 1999. Interactive ray tracing for volume visualization. *IEEE Trans. on Computer Graphics and Visualization 5* (3), 238–250.

PARKER, S. G., MARTIN, W., SLOAN, P.-P. J., SHIRLEY, P., SMITS, B. E., AND HANSEN, C. D. 1999. Interactive ray tracing. In *Proceedings of Interactive 3D Graphics*, 119–126.

PURCELL, T., BUCK, I., MARK, W., AND HANRAHAN, P. 2002. Ray tracing on programmable graphics hardware. In *Proceedings of SIGGRAPH*, 703–712.

REINHARD, E., SMITS, B., AND HANSEN, C. 2000. Dynamic acceleration structures for interactive ray tracing. In *Proceedings of the Eurographics Workshop on Rendering*, 299–306.

RESHETOV, A., SOUPIKOV, A., AND HURLEY, J. 2005. Multi-level ray tracing algorithm. In *Proceedings of ACM SIGGRAPH*, 1176–1185.

SPACKMAN, J., AND WILLIS, P. 1991. The SMART navigation of a ray through an oct-tree. *Computers and Graphics 15* (2), 185–194.

SPACKMAN, J. 1990. *Scene Decompositions for Accelerated Ray Tracing*. PhD thesis, The University of Bath, UK. Available as Bath Computer Science Technical Report 90/33.

STOLL, G., MARK, W. R., DJEU, P., WANG, R., AND ELHASSAN, I. 2006. Razor: An Architecture for Dynamic Multiresolution Ray Tracing. Tech. Rep. 06-21, University of Texas at Austin Dep. of Comp. Science.

STOLL, G. 2005. Part II: Achieving Real Time - Optimization Techniques. In *SIGGRAPH 2005 Course on Interactive Ray Tracing*, P. Slusallek, P. Shirley, I. Wald, G. Stoll, and B. Mark, Eds.

WALD, I., AND HAVRAN, V. 2006. On building good kd-trees for ray tracing, and on doing this in O(N log N). Tech. Rep. UUSCI-2006-009, SCI Institute, University of Utah.

WALD, I., SLUSALLEK, P., BENTHIN, C., AND WAGNER, M. 2001. Interactive Rendering with Coherent Ray Tracing. *Computer Graphics Forum 20* (3), 153–164. (Proceedings of Eurographics).

WALD, I., BENTHIN, C., AND SLUSALLEK, P. 2003. Distributed Interactive Ray Tracing of Dynamic Scenes. In *Proceedings of the IEEE Symposium on Parallel and Large-Data Visualization and Graphics (PVG)*.

WALD, I., BOULOS, S., AND SHIRLEY, P. 2006. Ray Tracing Deformable Scenes using Dynamic Bounding Volume Hierarchies. *ACM Transactions on Graphics (conditionally accepted, to appear)*.

WALD, I. 2004. *Realtime Ray Tracing and Interactive Global Illumination*. PhD thesis, Saarland University.

WOOP, S., SCHMITTLER, J., AND SLUSALLEK, P. 2005. RPU: A programmable ray processing unit for realtime ray tracing. In *Proceedings of SIGGRAPH*, 434–444.